

# Gateable Nanofluidic Interconnects for Multilayered Microfluidic Separation Systems

Tzu-Chi Kuo,<sup>†,‡</sup> Donald M. Cannon, Jr.,<sup>‡</sup> Yanning Chen,<sup>†</sup> Joseph J. Tulock,<sup>†,‡</sup> Mark A. Shannon,<sup>‡,§</sup> Jonathan V. Sweedler,<sup>\*,†,‡</sup> and Paul W. Bohn<sup>\*,‡</sup>

Department of Chemistry, Department of Mechanical Engineering, and Beckman Institute for Advanced Science and Technology, University of Illinois at Urbana–Champaign, 600 South Mathews Avenue, Urbana, Illinois 61801

**The extension of microfluidic devices to include three-dimensional fluidic networks allows complex fluidic and chemical manipulations but requires innovative methods to interface fluidic layers. Externally controllable interconnects, employing nuclear track-etched polycarbonate membranes containing nanometer-diameter capillaries, are described that produce hybrid three-dimensional fluidic architectures. Controllable nanofluidic transfer is achieved by controlling applied bias, polarity, and density of the immobile nanopore surface charge and the impedance of the nanocapillary array relative to the microfluidic channels. Analyte transport between vertically separated microchannels has three stable transfer levels, corresponding to zero, reverse, and forward bias. The transfer can even depend on the properties of the analyte being transferred such as the molecular size, illustrating the flexible character of the analyte transfer. In a specific analysis implementation, nanochannel array gating is applied to capillary electrophoresis separations, allowing selected separated components to be isolated for further manipulation, thereby opening the way for preparative separations at attomole analyte mass levels.**

Fully integrating the broad range of powerful molecular separations and other forefront technologies<sup>1–20</sup> with microfluidics

would make it possible to subject tiny analytical samples to complex sequences of chemical manipulations, thereby enabling true multidimensional chemical analysis at heretofore unattainably low sample levels. For example, preparative separations are difficult using microfluidics, because sample collection in electrophoretic microdevices is cumbersome and implementing valves at collection vials involves considerable complexity in a two-dimensional format. Extension of microfluidic devices to three dimensions allows complex solution handling such as preparation, separation, tagging, or affinity recognition in a given plane followed by transfer to a different plane for further processing and manipulations. Gated transfer could be used to collect bands separated by chip-based electrophoresis for further processing or characterization, thereby creating preparative forms of chromatography operating at the attomole level. Furthermore, such multilevel microfluidic structures parallel the massively three-dimensional architectures characteristic of electronic devices and open the way for complex fluidic manipulations. However, the creation of true multilevel fluidic devices has proven to be a challenging task. Early examples of multilayer microfluidic flow designs consisted of stacked modules with relatively large volume tubes as the interlayer interconnect for the realization of a micro total analysis system.<sup>21–23</sup> Other examples of three-dimensional

\* Corresponding authors. E-mail: sweedler@scs.uiuc.edu; bohn@scs.uiuc.edu.

<sup>†</sup> Department of Chemistry.

<sup>‡</sup> Beckman Institute for Advanced Science and Technology.

<sup>§</sup> Department of Mechanical Engineering.

- (1) Terry, S. C.; Jerman, J. H.; Angell, J. B. *IEEE Trans. Electron Devices* **1979**, *ED-26*, 1880–1886.
- (2) Manz, A.; Graber, N.; Widmer, H. M. *Sens. Actuators, B* **1990**, *1*, 244–248.
- (3) Harrison, D. J.; Fluri, K.; Seiler, K.; Fan, Z.; Effenhauser, C. S.; Manz, A. *Science (Washington, D. C.)* **1993**, *261*, 895–897.
- (4) Seiler, K.; Fan, Z. H. H.; Fluri, K.; Harrison, D. J. *Anal. Chem.* **1994**, *66*, 3485–3491.
- (5) Jacobson, S. C.; Hergenroder, R.; Koutny, L. B.; Warmack, R. J.; Ramsey, J. M. *Anal. Chem.* **1994**, *66*, 1107–1113.
- (6) Jacobson, S. C.; McKnight, T. E.; Ramsey, J. M. *Anal. Chem.* **1999**, *71*, 4455–4459.
- (7) Woolley, A. T.; Mathies, R. A. *Proc. Natl. Acad. Sci. U.S.A.* **1994**, *91*, 11348–11352.
- (8) Haab, B. B.; Mathies, R. A. *Anal. Chem.* **1999**, *71*, 5137–5145.
- (9) Koch, M.; Schabmueller, C. G. J.; Evans, A. G. R.; Brunnschweiler, A. *Sens. Actuators, A* **1999**, *74*, 207–210.
- (10) Jaeggi, D.; Gray, B. L.; Mourlas, N. J.; van Driehhuizen, B. P.; Williams, K. R.; Maluf, N. I.; Kovacs, G. T. A. *Transducer Res. Found., Cleveland, OH*. 1998; pp 112–115.

- (11) Man, P. F.; Mastrangelo, C. H.; Burns, M. A.; Burke, D. T. *Proc. –IEEE Annu. Int. Workshop Micro Electro Mech. Syst.*, 11th; New York, 1998; pp 45–50.
- (12) Yang, X.; Yang, J. M.; Tai, Y.-C.; Ho, C.-M. *Sens. Actuators, A* **1999**, *73*, 184–191.
- (13) Christel, L. A.; Petersen, K.; McMillan, W.; Kovacs, G. T. A. *Transducer Res. Found., Cleveland, OH*, 1998; pp 363–366.
- (14) Folch, A.; Ayon, A.; Hurtado, O.; Schmidt, M. A.; Toner, M. *J. Biomech. Eng.* **1999**, *121*, 28–34.
- (15) Becker, H.; Gartner, C. *Electrophoresis* **2000**, *21*, 12–26.
- (16) Lee, L. P.; Berger, S. A.; Liepmann, D.; Pruitt, L. *Sens. Actuators, A* **1998**, *71*, 144–149.
- (17) Martin, P. M.; Matson, D. W.; Bennett, W. D.; Hammerstrom, D. J. *Proc. SPIE-Int. Soc. Opt. Eng.* **1998**, *3515*, 172–176.
- (18) Duffy, D. C.; Schueller, O. J. A.; Brittain, S. T.; Whitesides, G. M. *J. Micromech. Microeng.* **1999**, *9*, 211–217.
- (19) McDonald, J. C.; Duffy, D. C.; Anderson, J. R.; Chiu, D. T.; Wu, H. K.; Schueller, O. J. A.; Whitesides, G. M. *Electrophoresis* **2000**, *21*, 27–40.
- (20) Philpott, M. L.; Beebe, D. J.; Fischer, A.; Flachsbar, B.; Marshall, M.; Miller, N. R.; Selby, J. C.; Shannon, M. A.; Wu, Y. *2000 Solid-State Sensors and Actuators Workshop*, Hilton Head Island, SC, June 4–8 2000; pp 226–229.
- (21) van der Schoot, B. H.; Jeanneret, S.; van den Berg, A.; de Rooij, N. F. *Sens. Actuators, B* **1992**, *6*, 57–60.
- (22) Fetting, J. C.; Manz, A.; H., L.; Widmer, H. M. *Sens. Actuators, B* **1993**, *17*, 19–25.
- (23) Verpoorte, E. M. J.; Van der Schoot, B. H.; Jeanneret, S.; Manz, A. *J. Micromech. Microeng.* **1994**, *4*, 246–256.

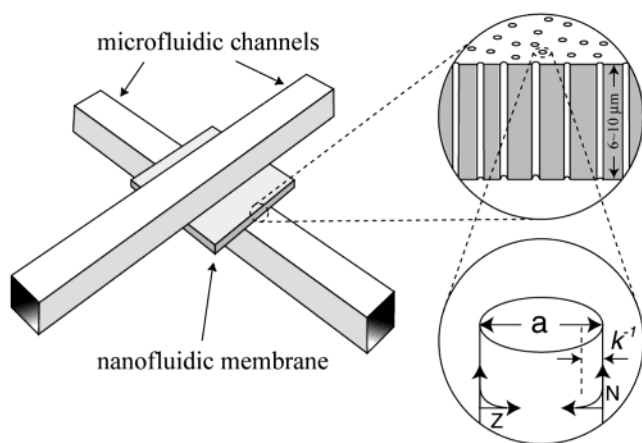


Figure 1. Upper left: Schematic diagram of the crossed microfluidic channels separated by a nanometer-diameter capillary array interconnect (light gray at intersection). Upper right: The cross-sectional schematic of the nanocapillary array illustrates the large aspect ratios characteristic of the nanopores employed. Typical length-to-width ratios were in the range 20–350 for the nanocapillaries used in this work. Lower right: Schematic diagram showing relative sizes of the channel diameter ( $a$ ) and Debye length ( $\kappa^{-1}$ ) typically encountered with nanometer diameter channels and millimolar electrolyte solutions.  $Z$  is the distance from the nanochannel wall, and  $N$  is the ion number density.

flow patterns used discrete microchannels to bridge, rather than connect, independent microfluidic channels for the alleviation of space constraints.<sup>24–26</sup> Topologically complex systems have led to microvalves and micromixers<sup>27,28</sup> and even pressure-actuated valves.<sup>29</sup>

Described here is an extension of fluidic circuitry that can exploit the third dimension using a nanofluidic gateable (externally controllable) interconnect between microfluidic layers. Nanometer-diameter capillary arrays commercially available as nanoporous membranes containing 15–200-nm-diameter cylindrical pores are employed as interconnects to establish controllable fluidic communication between micrometer-scale channels operating in vertically separated planes (Figure 1). Fluidic communication can be established among any number of vertically stacked planes with the nanochannel arrays acting as an electrically controlled nonmoving valve between the layers. These interconnects provide controllable transport of components at the desired point in space and time between the functional layers, thus allowing diverse separation modes to be used in a single device.

In nanometer-diameter capillaries, flow occurs in structures of the same size as physical parameters that govern the flow. For example, the Debye length,  $\kappa^{-1}$  (Figure 1), which characterizes

the length scale of ionic interactions in solution, spans the range  $1 \text{ nm} < \kappa^{-1} < 50 \text{ nm}$  when the ionic strength of the buffer solution lies in the high-to-low millimolar range.<sup>30</sup> In nanofluidic devices, the capacity factor,  $K$ , governed by the surface-to-volume ratio, can be orders of magnitude larger than in the corresponding microfluidic analogs. Furthermore, the nanopores themselves can be operated to effect molecular separations. Surface charge density,  $\sigma_s$ , is a critical property influencing these phenomena,<sup>31,32</sup> because the enhanced surface-to-volume ratio in these nanofluidic channels means that a significant fraction of the total charge is bound to the walls and is immobile. Because it determines the magnitude of the surface potential and the applicability of the Debye–Hückel approximation, surface charge density provides an experimental handle to adjust the microscopic processes that determine transport in the nanopore. Martin et al. previously showed how ion permselective membranes could be constructed from electroless Au-coated channels in nuclear track-etched membranes,<sup>33</sup> thus opening the way for the use of electroless Au deposition followed by self-assembly to fabricate structures that can mediate molecular transport.<sup>34–40</sup> Thus, facile control of nanofluidic flow achieved by varying the bias, nanochannel wall charge density, nanochannel diameter, charge polarity, and/or solution ionic strength offers the opportunity to effect intelligent transfer of fluid components.

## EXPERIMENTAL SECTION

**Materials.** Fluorescein disodium salt ( $\text{Fl}^{2-}$ ), fluorescein isothiocyanate (FITC), L-arginine, L-glutamate, and FITC-labeled dextrans were used as received from Sigma. 4,4-Difluoro-5,7-dimethyl-4-bora-3a,4a-diaza-s-indacene-3-succinimidylpropionate (bodipy, BO-DIPY FL, SE, Molecular Probes) was used as received. Deionized  $\text{H}_2\text{O}$  (18.2  $\text{M}\Omega \text{ cm}$ ) from a Milli-Q UV-Plus system (Millipore) was used to prepare all solutions. Phosphate buffer solutions were prepared from mono-, di-, and tribasic potassium phosphate salts (Aldrich) and were adjusted to proper pH values with 0.1 M NaOH or HCl. Stock solutions of arginine and glutamate were prepared in a 10 mM sodium tetraborate buffer (pH 8.6) and were derivatized with FITC at 100:1 mole ratio at room temperature in the dark for at least 24 h. Nucleopore polycarbonate track-etched (PCTE, with poly(vinylpyrrolidone) coating) membranes were used as received from Osmonics. These membranes were 6–10  $\mu\text{m}$  thick typically, depending on pore size.<sup>17</sup> These membranes have highly monodisperse distributions of pores with pore densities of  $3 \times 10^8 \text{ cm}^{-2} < N_p < 6 \times 10^8 \text{ cm}^{-2}$ , depending on pore diameter.

- (24) Anderson, J. R.; Chiu, D. T.; Jackman, R. J.; McDonald, J. C.; Wu, H.; Whitesides, S. H.; Whitesides, G. M.; Cherniavskaya, O. *Anal. Chem.* **2000**, *72*, 3158–3164.
- (25) Chiu, D. L.; Pezzoli, E.; Wu, H.; Stroock, A. D.; Whitesides, G. M. *Proc. Natl. Acad. Sci. U.S.A.* **2001**, *98*, 2961–2966.
- (26) Chiu, D. T.; Li Jeon, N.; Huang, S.; Kane, R. S.; Wargo, C. J.; Choi, I. S.; Ingber, D. E.; Whitesides, G. M. *Proc. Natl. Acad. Sci. U.S.A.* **2000**, *97*, 2408–2413.
- (27) González, C.; Smith, R. L.; Howitt, D. G.; Collins, S. D. *Sens. Actuators, A* **1998**, *66*, 315–322.
- (28) Gray, B. L.; Jaeggi, D.; Mourlas, N. J.; van Driehuisen, B. P.; Williams, K. R.; Maluf, N. I.; Kovacs, G. T. A. *Sens. Actuators, A* **2000**, *77*, 57–65.
- (29) Kugelmass, S. M.; C., L.; DeWitt, S. H. *Proc. SPIE-Int. Soc. Opt. Eng.* **1999**, *3877*, 88–94.

- (30) Rice, C. L.; Whitehead, R. *J. Phys. Chem.* **1965**, *69*, 4017–4024.
- (31) Fair, J. C.; Osterle, J. F. *J. Chem. Phys.* **1971**, *54*, 3307–3316.
- (32) Martínez, L.; Gigosos, M. A.; Hernandez, A.; Tejerina, F. *J. Membr. Sci.* **1987**, *35*, 1–20.
- (33) Nishizawa, M.; Menon, V. P.; Martin, C. R. *Science (Washington, D. C.)* **1995**, *268*, 700–702.
- (34) Jirage, K. B.; Hulteen, J. C.; Martin, C. R. *Anal. Chem.* **1999**, *71*, 4913–4918.
- (35) Hulteen, J. C.; Jirage, K. B.; Martin, C. R. *J. Am. Chem. Soc.* **1998**, *120*, 6603–6604.
- (36) Hou, Z. Z.; Abbott, N. L.; Stroeve, P. *Langmuir* **2000**, *16*, 2401–2404.
- (37) Hou, Z.; Abbott, N. L.; Stroeve, P. *Langmuir* **1998**, *14*, 3287–3297.
- (38) Ito, Y.; Park, Y. S.; Imanishi, Y. *Langmuir* **2000**, *16*, 5376–5381.
- (39) Bluhm, E. A.; Bauer, E.; Chamberlin, R. M.; Abney, K. D.; Young, J. S.; Jarvinen, G. D. *Langmuir* **1999**, *15*, 8668–8672.
- (40) Bluhm, E. A.; Schroeder, N. C.; Bauer, E.; Fife, J. N.; Chamberlin, R. M.; Abney, K. D.; Young, J. S.; Jarvinen, G. D. *Langmuir* **2000**, *16*, 7056–7060.

**Device Fabrication.** Crossed microfluidic channels were fabricated from poly(dimethylsiloxane) (PDMS) in planes above and below the nanoporous membrane. Microfluidic channels were fabricated using standard rapid prototyping protocols for PDMS.<sup>19</sup> PDMS was treated in O<sub>2</sub> plasma to facilitate sealing. Assembly was accomplished by placing a 10 mm × 1 mm section of membrane centered on the bottom PDMS channel and then placing the top PDMS channel at 90° to the bottom channel within the area of the membrane. Sealing was affected by the portions of the PDMS monoliths on the periphery of the membrane. Channels used in the experiments described here were 100 μm wide, 60 μm deep, and 14 mm long for the transport devices and 50 μm wide and 25 μm deep for the electrophoresis separation devices. A reservoir PDMS layer was sealed on the top of the sandwiched device.

**Transport Control and Measurement.** Microfluidic transport was achieved through applying bias across different reservoirs. Potentials were applied across the PDMS channels and the nanocapillary array junction via remote Pt electrodes inserted in the reservoirs, and applied voltages are given throughout as  $\Delta V$  ( $= V_{\text{rec}} - V_{\text{source}}$ ). An eight-relay system was used to switch electrical contact between electrodes and voltage source at different configurations for microfluidic manipulation. Transport control was monitored with either single-spot or dual-spot epilluminated laser-induced fluorescence (LIF) and fluorescence microscopic imaging of fluid streams containing fluorophores by interrogating the fluorescence signal on either the source or the receiving channel side of the nanofluidic membrane. The LIF system consists of one or two of the following modules. The 488-nm radiation of an Ar<sup>+</sup> laser (Innova 300, Coherent) was focused by a 10× objective onto a 50-μm spot in the interrogated channel, and the fluorescence was collected by the same objective and detected by a photon counting PMT (HC124, Hamamatsu USA). Dichroic mirrors (505DCLP, Chroma) and band-pass filters (525 nm/50-nm wide, HQ525/50m, Chroma) were used in these epi LIF systems. Controls of the relay system and PMT data collection were achieved through a computer with LabVIEW programs and data acquisition cards (National Instruments). An inverted fluorescence microscope (Axiovert 100, Zeiss) was used for imaging with a color CCD camera (Photometrics CoolSNAP fx, Roper Scientific).

## RESULTS AND DISCUSSION

The crossed microfluidic channels shown in Figure 1 spatially define the transport region and eliminate the need for precise alignment of the membrane containing the nanocapillary array. Figure 2 shows a photograph of a separation/collection device. The small white rectangle is the PCTE membrane containing the 200-nm-diameter cylindrical pores, and the vertical channel overlapping the membrane is the collection channel. For molecular transport studies, a two-channel (a simple cross) device was used with identical channels on both sides of the membrane (picture not shown). Analyte transport is interrogated by monitoring the transport of a fluorescently labeled probe on either the source or the receiving channel side of the nanofluidic membrane array. Figure 3a shows the transfer of the anionic fluorophore, fluorescein, across a 200-nm pore diameter nuclear track-etched polycarbonate (PCTE) capillary array to a buffer-filled receiving channel held at ground potential in the off state. Successive

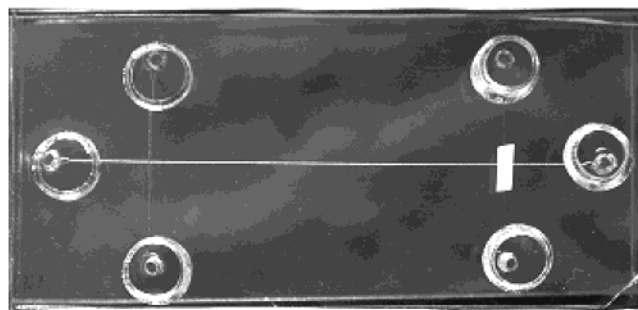


Figure 2. Photograph of a separation/collection microchip showing the crossed microchannels and the nanofluidic capillary array membrane.

transfers are affected by application of negative bias pulses. The fluorophore concentration probed during bias application is a balance between active transport from the source channel and diffusion along the receiving channel. When the bias is removed, diffusion depletes the concentration in the region probed, but with successive forward bias applications, the length of the receiving channel occupied by the probe increases, thereby diminishing the effect of diffusional dilution in subsequent transfers. In a similar experiment (Figure 3b), directional flow is maintained in the receiving channel. The buildup to steady state at the gating region after bias application, clearly more gradual than that without flow, results from the balance between active transport of the analyte across the nanofluidic array and its removal by cross-flow in the receiving channel. An obvious time offset is observed when the detection region is moved downstream of the interconnect (Figure 3b bottom trace). Figure 4a demonstrates the level of control and speed of transfer possible with these nanofluidic interconnects. Measurements on the changing edges of Figure 4a indicate steady-state concentration is reestablished in the receiving channel within ~1.2 s of applying the switching voltage. Figure 4b demonstrates the insensitivity to analyte charge state by comparing the transfer of the neutral fluorophore bodipy. While similarly designed crossed microfluidic arrays were recently demonstrated by Whitesides and co-workers,<sup>41</sup> these used passive diffusion through the pores of the polycarbonate membrane to mix the fluids, as opposed to the electrically driven flow demonstrated here.<sup>42–44</sup>

A significant advantage of using electrically driven flow, by choosing the pore diameter, pore surface chemistry, channel surface charge, and solution ionic strength, one can select the direction that fluid flows through the pore for the same externally applied voltage. Interestingly, in the microfluidic–nanofluidic hybrid architecture, the flow is opposite to the direction based on the electroosmotic flow characteristics of the 200-nm pore diameter PCTE capillary array alone.<sup>45</sup> The surfaces of the PCTE membrane channels are coated with poly(vinylpyrrolidone) (PVP)

- (41) Ismagilov, R. F.; Ng, J. M. K.; Kenis, P. J. A.; Whitesides, G. M. *Anal. Chem.* **2001**, 5207–5213.
- (42) Kuo, T.-C.; Cannon, D. M., Jr.; Feng, W.; Shannon, M. A.; Sweedler, J. V.; Bohn, P. W. *Micro Total Analysis Systems 2001*; Monterey, CA, October 21–25, 2001; Kluwer Academic Publishers: Dordrecht, 2001; pp 60–62.
- (43) Kuo, T.-C.; Cannon, D. M., Jr.; Shannon, M. A.; Bohn, P. W.; Sweedler, J. V. *Sens. Actuators, Phys.* **2003**, 102, 223–233.
- (44) Spencer, M. G.; Flachsbar, B. R.; Yasunaga, T.; Kuo, T.-C.; Sweedler, J. V.; Bohn, P. W.; Shannon, M. A. *Micro Total Analysis Systems 2001*; Monterey, CA, October 21–25, 2001; Kluwer Academic Publishers: Dordrecht, 2001; pp 195–196.

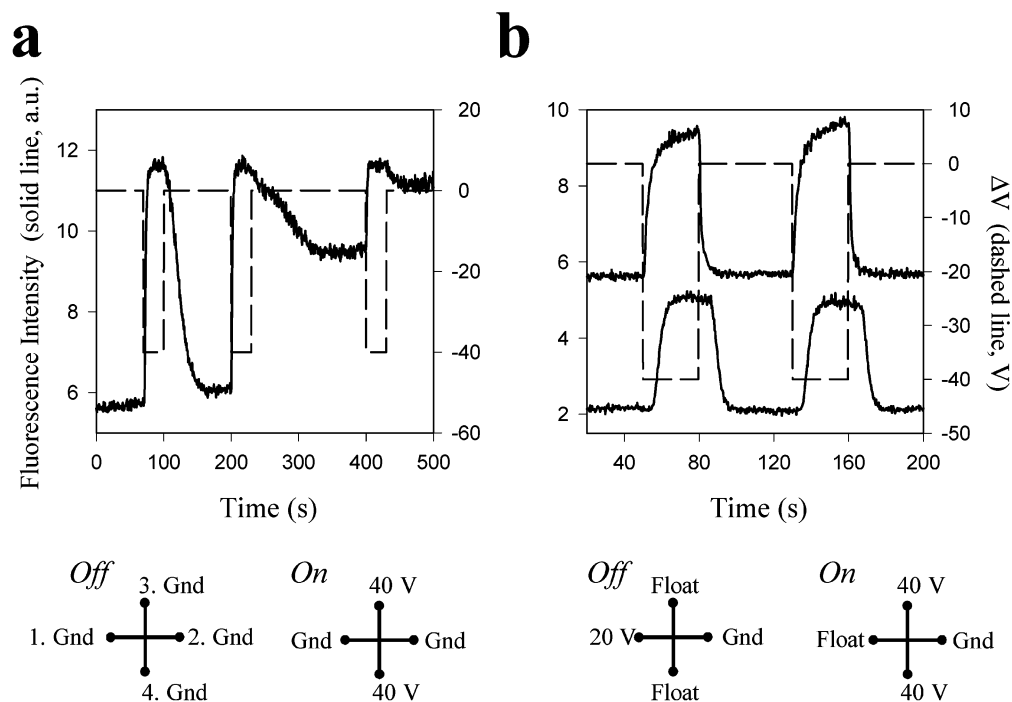


Figure 3. Fluorescence intensity (left ordinate, solid line) and applied bias,  $\Delta V$ , (right ordinate, dashed line) as a function of time showing transport of  $0.17 \mu\text{M}$  fluorescein in  $5 \text{ mM}$  pH 8 phosphate buffer (PB) across a  $200\text{-nm}$  pore diameter PCTE membrane. The schematics below the respective graphs show the bias voltage application schemes. Contacts 1 and 2 are in the receiving (horizontal) channel; contacts 3 and 4 are in the source (vertical) channel. (a) The receiving channel was held under flow-free conditions during the off state in this experiment. Detection was at the gate intersection in the receiving channel. (b) On and off bias potentials were designed to produce flow in the receiving channel. LIF detection was (upper trace) at the gating region in the receiving channel and (lower trace)  $100 \mu\text{m}$  downstream of the gating region in the receiving channel.

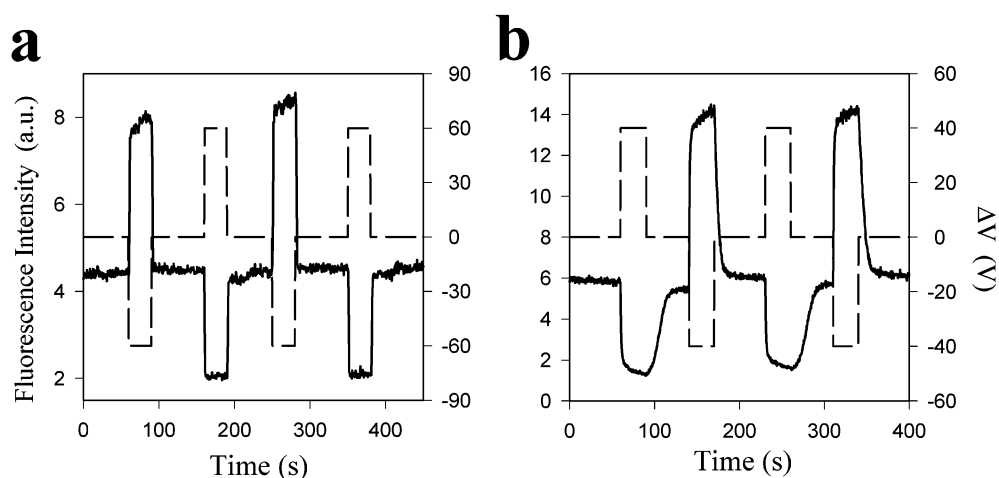


Figure 4. Fluorescence intensity (left ordinate, solid line) and applied bias,  $\Delta V$ , (right ordinate, dashed line) as a function of time showing transport across a  $200\text{-nm}$  pore diameter PCTE membrane. The bias potential configurations are similar to that of Figure 3 and are described in detail in the text. (a) Transport of  $0.17 \mu\text{M}$  fluorescein in  $5 \text{ mM}$  pH 8 PB. (b) Neutral probe transport using  $0.9 \mu\text{M}$  bodipy fluorophore (4,4-difluoro-5,7-dimethyl-4-bora-3a,4a-diaza-s-indacene-3-succinimidylpropionate) in  $5 \text{ mM}$  pH 8 PB.

to render them hydrophilic. The tertiary amine of the PVP is susceptible to protonation, making the surface net positive at pH 8, thus recruiting a population of negative solution counterions to the interior of the nanochannels. Under the low ionic strength conditions used here, the ionic population in the channel is predominantly  $\text{H}_2\text{PO}_4^-/\text{HPO}_4^{2-}$ , so forward bias is obtained with  $V_{\text{rec}} - V_{\text{source}} > 0$ , if the nanofluidic channels control the direction

of transport. Instead, flow in the direction predicated on the (negative) charge state of the PDMS surfaces of the microfluidic channels controls transport. Figure 5 demonstrates that the direction of flow is reversed for transport across a  $200\text{-nm}$  pore diameter array (a, left) compared with that across a  $15\text{-nm}$  pore diameter capillary array (a, right). This behavior can be understood based on two effects—the greatly increased resistance to pressure-driven flow through the smaller pores and the greater voltage drop across the pores in the  $15\text{-nm}$ -diameter case.

(45) Kuo, T.-C.; Sloan, L. A.; Sweedler, J. V.; Bohn, P. W. *Langmuir* **2001**, *17*, 6298–6303.

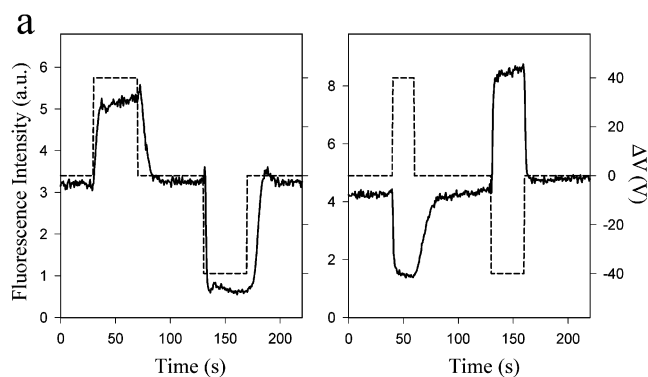


Figure 5. (a) Migration of a probe across PCTE capillary arrays with 15- (left) and 200-nm (right) pore diameters connecting two 100- $\mu\text{m}$ -wide PDMS channels. Fluorescence intensity and applied bias  $\Delta V$  as a function of time to monitor the transport of 0.17  $\mu\text{M}$  fluorescein in 5 mM pH 8 PB. (b) An impedance network model for the combined microfluidic (source and receiving) and nanofluidic channels ( $R_m$ ).

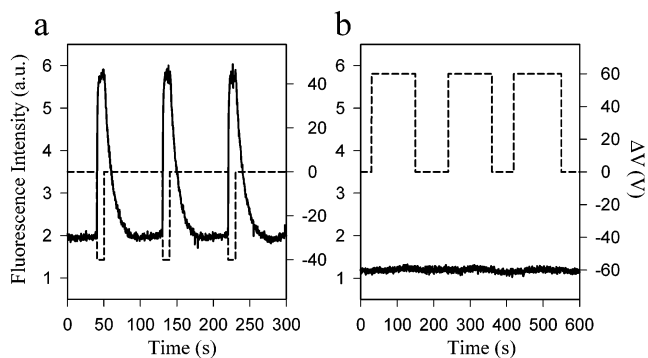


Figure 6. Electrokinetic macromolecular transport of 2-MDa FITC-labeled dextrans (40 nM) in 5 mM pH 8 PB across (a) 200- and (b) 15-nm pore diameter PCTE membrane arrays.

Modeling the impedance network for a three-dimensional device with two microfluidic channels and a 200-nm pore diameter interconnect (Figure 5b) shows that  $<2\%$  of the potential is dropped across the nanofluidic array. However, for 15-nm pore diameters,  $\sim 25\%$  of the potential drops across the array, so that the PCTE nanopore electroosmotic flow dominates fluid transport when 15-nm pore diameters are used, but not when larger pores are employed.

Results in Figures 3–5 demonstrate the diodelike fluidic manipulation possible with nanoporous interconnects. However, the flow control is much richer than that available to electronic circuitry, since flow can also be controlled to achieve intelligent analyte transfer based on molecular properties, e.g., molecular size. Mass-independent transport, critical for simple nondiscriminate valving of macromolecular transport, is observed in the 200-nm pore diameter interconnects for FITC-labeled dextrans at all molecular masses up to and including 2 MDa (Figure 6a). Conversely, the smaller 15-nm pore diameter capillary arrays exhibit a mass-dependent transfer of analyte, shown by complete inhibition of transport for 2-MDa dextrans (Figure 6b). The molecular size separation cutoff of  $\sim 10$  kDa is determined by

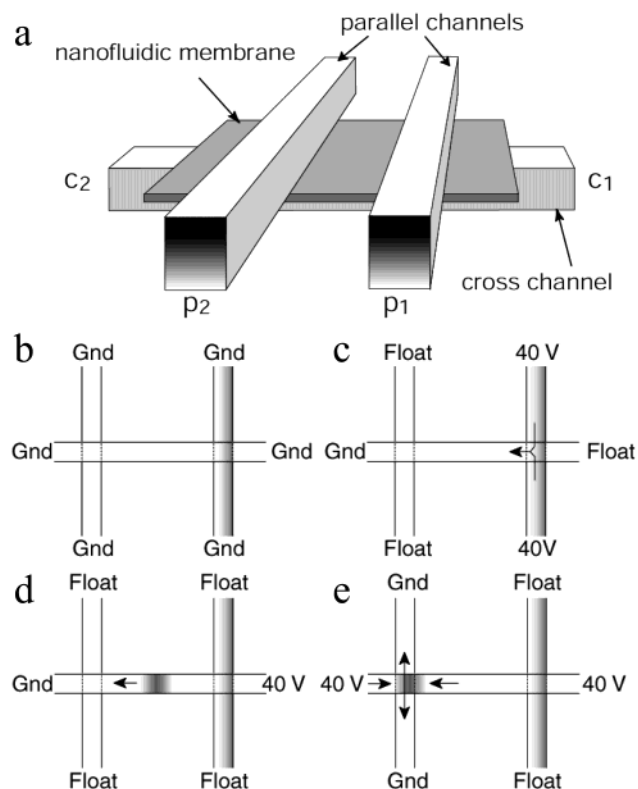


Figure 7. (a) Schematic of the parallel–cross channel system (not to scale). The parallel channels  $p_1$  and  $p_2$  are embedded in the upper PDMS layer, separated by a 200-nm pore diameter PCTE membrane capillary array from a cross channel,  $c$ , in the lower PDMS layer. (b–e) Bias configurations for grounding (b), injection (c), flowing in channel  $c$  (d), and collection (e).

experiments with a series of dextrans with this 15-nm pore diameter capillary array interconnect configuration (data not shown). The ability to design interconnects that add molecular specificity, such as the size-based effect demonstrated here, adds great flexibility to three-dimensional fluidic devices.

If an additional microfluidic channel is added, yielding two parallel channels intersecting a cross channel, then the device can both inject a sample and collect the analyte. The schematic of this device is shown in Figure 7a. By switching the voltage bias configurations (Figure 7b–e), a versatile fluidic manipulation was demonstrated. Figure 8 shows a sequence of fluorescence images from injection to collection obtained using this device. In these images, fluorescein solution is electrokinetically injected into the cross channel; subsequently, the electrical configuration is switched to move the fluorescein band along the cross channel. Knowing the velocity in the cross channel and the injection time allows timing the forward bias pulse at the next channel intersection to move the band vertically into the collection channel. After reversing the bias, a slight broadening of the captured band is observed, attributed to diffusion. Selective transport of a single band out of multiple repeated injections is achieved in the same fashion, ensuring the preparative manipulations envisioned above can be realized.

These multilayered fluidic control concepts are used to accomplish preparative separations on the microscale by incorporating them into a microfabricated electrophoresis system for the actively controlled transfer of a specific analyte from the main

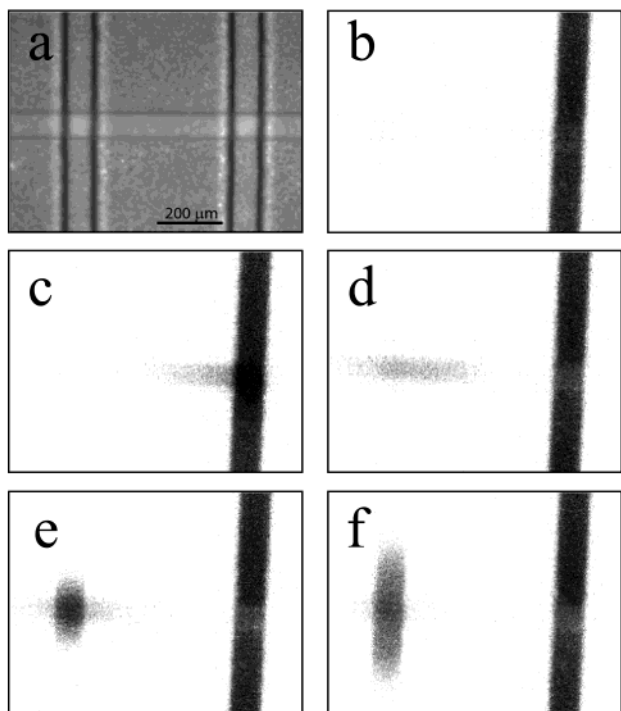


Figure 8. Injection and collection with the parallel-cross channel system. (a) White light image of the interrogated area. (b-f) Fluorescence images of the injection/collection sequence. Channel  $p_1$  as filled with  $2 \mu\text{M}$  fluorescein $^{2-}$  in  $5 \text{ mM}$  pH 9 PB, and the channels  $c$  and  $p_2$  were filled with  $5 \text{ mM}$  pH 9 PB initially. (b) All reservoirs grounded. (c) Injection with  $40\text{-V}$  bias across  $p_1$ - $c$  junction. (d) Moving the injected band in the cross channel with  $40\text{-V}$  bias between  $c_1$  and  $c_2$ . (e) Collection of the fluorescein band with  $40\text{-V}$  bias applied to the  $c$ - $p_2$  junction. (f) Collection voltage off, but  $40\text{-V}$  bias was applied between  $c_1$  and  $c_2$  to maintain flow. The entire sequence of micrographs spanned 12 s.

separation channel into a second channel. A nanofluidic capillary array is placed between two microchannel layers at the end of the main separation channel (Figures 2 and 9, top), and the process is monitored by fluorescence measurements in two detection zones located before and after the gating (nanofluidic interconnect) region. Figure 9 shows four successive separations of a mixture of amino acids derivatized with FITC, recorded by the postgate detection. When the gate is off (Figure 9a), the system acts as a standard electrophoresis device; when the nanocapillary gate is forward biased, the analyte is transported to the vertically displaced receiving channel as it passes the gate region, and that particular analyte signal is eliminated from the postgate detection region. The gate pulse can be activated to switch a selected analyte band (or bands) completely from the main electrophoresis channel into the collection channel. In Figure 9b, the gating pulse is timed to remove the first analyte band, fluorescein thiohydantoin-glutamate, and complete separation of this band from the main channel flow is accomplished. The mass that is captured in this experiment is  $\sim 10^{-16}$  mol. Subsequently, with selective triggering optimized for each analyte band, the two peaks corresponding to the two separate fluorescein thiohydantoin-arginine bands are sequentially separated from the main flow (Figure 9c,d). The selective sampling of the nonresolved arginine bands demonstrates that picoliter-volume analyte bands can be sampled in a preparative sense with these three-dimensional hybrid nanofluidic/microfluidic devices.

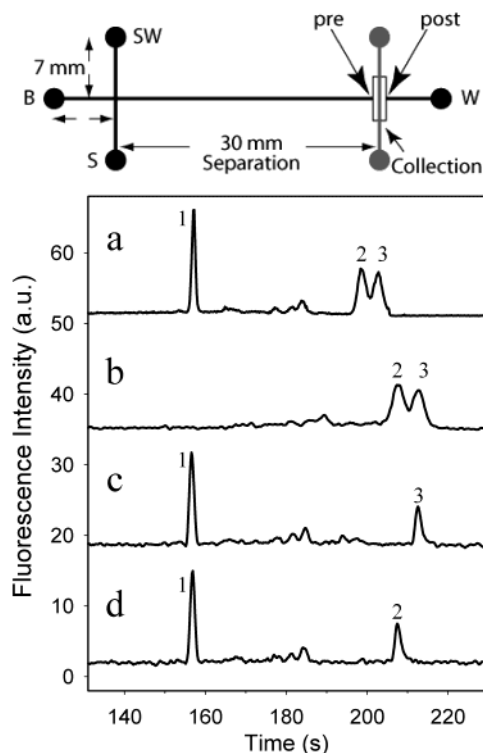


Figure 9. Separation and selective collection of arginine and glutamate derivatized with FITC. Schematic on the top shows the sampling geometry, i.e., a capillary electrophoresis microchip (black) coupled with a molecular gate collection channel (gray). Laser-induced fluorescent signals were monitored before and after the membrane gate, as indicated with the arrows, with the data shown here recorded from the aftergate detector. The electropherogram shown in (a) was obtained for a separation where no collection was performed. For selective collection experiments (b-d), the gate collection state was activated for a period matching the analyte bandwidth as judged from (a). The electropherograms demonstrate the separation and selective collection of three bands: glutamate (b); first arginine band (c); and a second arginine band (d). The difference in elution times between the nongated and gated experiments is from the actuation of the low-voltage gate located prior to the detection area affecting the elution time. Separations were based on electrophoretic mobility differences between anions, and the electrical field strength used for separation was  $170 \text{ V cm}^{-1}$ .

Gateable transfer of selected solution components between vertically separated microfluidic channels provides a simple solution to multilevel fluidic architectures. Integration of a single miniaturized component in the nanofluidic regime into a microfluidic device allows several limitations of electrophoretic devices to be circumvented. Diverse separation modalities can be realized within a single monolithic three-dimensional micro/nanofluidic device and can be based on externally controllable nondiscriminating transport or on transport biased according to charge, molecular weight, or times of elution. Preliminary experiments even indicate that gates can be used to concentrate analyte by optimizing temporal gating protocols and buffer composition. With careful choice of the nanometer-diameter capillary array physical properties in conjunction with the controlling voltages, a wide range of operational modes such as the nonselective and mass-selective analyte transfer modes demonstrated here can be incorporated into devices. Given the large variety of single-layer devices already optimized to perform cellular manipulations, chemical reactions,

and complex separations, the ability to integrate these individual components into multilayer structures with external control for the intelligent transfer of individually selectable analytes between layers will enable many heretofore unattainable applications.

#### ACKNOWLEDGMENT

This work was supported by the Department of Energy, by the Defense Advanced Research Projects Agency, and

by the National Cancer Institute. D.M.C. acknowledges the Beckman Institute for Advanced Science and Technology Fellows program.

Received for review July 19, 2002. Accepted February 19, 2003.

AC025958M